Improved Design of IPMSM for Sensorless Drive with Absolute Rotor Position Estimation Capability

Yong-Cheol Kwon, and Seung-Ki Sul
School of Electrical & Computer Engineering
Seoul National University
Seoul, Korea
dydcjfe@eepel.snu.ac.kr, sulsk@plaza.snu.ac.kr

Noor Aamir Baloch, Sohji Murakami, and Shinya Morimoto
Energy Conversion Technology Group
YASKAWA ELECTRIC CORPORATION
12-1 Otemachi, Kokurakita-ku, Kitakyushu 803-8530, JAPAN
baloch@yaskawa.co.jp, smurakam@yaskawa.co.jp,
sinya@yaskawa.co.jp

***Abstract*—In this paper, two designs of Interior Permanent Magnet Synchronous Machine (IPMSM) for sensorless drive with absolute rotor position estimation capability are proposed. A conventional IPMSM design prepared for the same purpose had a demerit that for absolute position estimation, saying that the rotor should initially stroke for 100° in the worst case. In order to reduce the initial stroke of the rotor, two new IPMSM designs featuring asymmetric winding and asymmetric rotor geometry are proposed and constructed as prototype motors. With the prototype motors, initial stroke of the rotor has been reduced to 30°. Moreover, basic characteristics of the motor such as torque ripples and harmonics of EMF have been also conspicuously improved. The overall performances of the proposed designs have been evaluated by rigorous finite element analysis and experimental test.**

Keywords—Permanent magnet synchronous machine, motor design, finite element method, sensorless drive, absolute rotor position estimation.

NOMENCLATURE

PP	number of pole-pairs.
θ_{rm}	absolute (mechanical) rotor position.
θ_r	electrical rotor position, $PP \cdot \theta_{rm}$.
$\hat{\theta}_{rm}$	estimated value of θ_{rm}.
$\hat{\theta}_r$	estimated value of θ_r.
λ_f	back-EMF constant.
R_s	winding resistance.
L_{ds}, L_{qs}	d-q components of stator self-inductance.

I. INTRODUCTION

Sensorless drive of Interior Permanent Magnet Synchronous Machine (IPMSM) has been developed for last two decades. Especially from zero to low speed range, saliency tracking method [1]-[3] has been widely used. Since spatial variation of inductance of IPMSM is clearly determined by the rotor position, the rotor position can be estimated by injecting additional High Frequency (HF) voltage signal and analyzing its resultant HF current ripple. Thanks to the development of signal injection and signal processing techniques, sensorless servo drive of IPMSM had been commercialized [4].

Despite the development of the signal injection sensorless control so far, most of them only addressed the estimation of the rotor position in electrical angle, not in mechanical angle. In common AC motor designs, inductance profile of motor is repeated for every electrical revolution, which makes absolute (mechanical) rotor position unidentifiable. Normally the electrical rotor position is enough in the application of the torque/speed control. However, in some applications such as control of robot arms and machine tools, absolute position should be identified and controlled.

Recently, a paper [5] had proposed an IPMSM design and its control algorithm for the estimation of the absolute rotor position. In the reference, an asymmetric IPMSM design with rotor trenches and irregular winding was proposed. By the stator and rotor asymmetries, synchronous inductance of IPMSM can be modulated according to the absolute rotor position. The modulated inductance can be reflected to HF current ripple induced by HF voltage injection, which can be exploited for identifying the absolute rotor position. However, the design and algorithm proposed in [5] required an initial stroke of the rotor, which was 100° in mechanical angle in the worst case. In robot and machine tool applications, such a large initial movement of the rotor could be unacceptable.

This paper proposes two IPMSM designs which are named as hole-type and shaving-type designs and control algorithm for the estimation of the absolute rotor position with the reduced initial stroke of the rotor. In the proposed designs, only rotor structures are modified from the conventional one in [5]. The basic performances of the proposed designs are evaluated through Finite Element Method (FEM) analysis and proven that the performance of the newly designed motor surpasses that of the motor in [5]. The motors based on two new designs have been actually constructed as prototype motors for experimental verification. It is experimentally proved that the initial stroke is reduced to 30° in the worst case.

978-1-4799-5784-2/14/$31.00©2014 IEEE

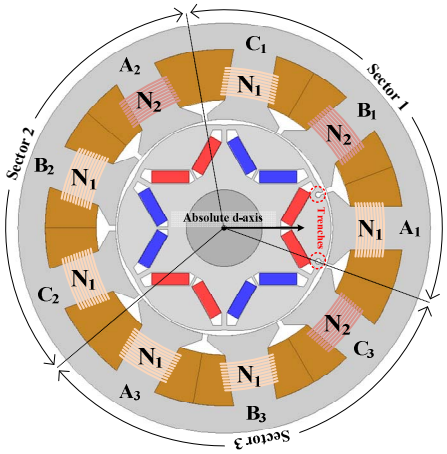

Figure 1. Conventional design.

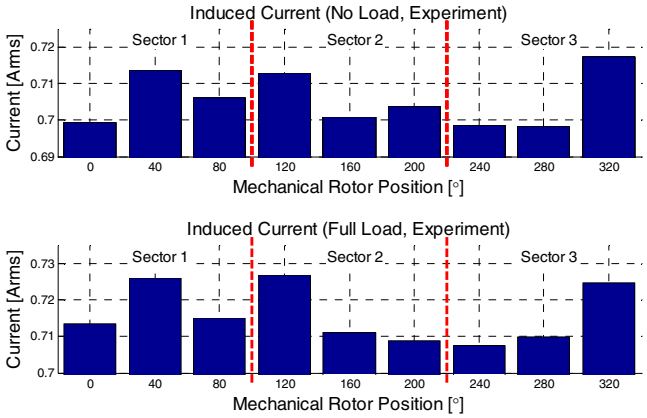

Figure 2. Induced current profiles (conventional design).

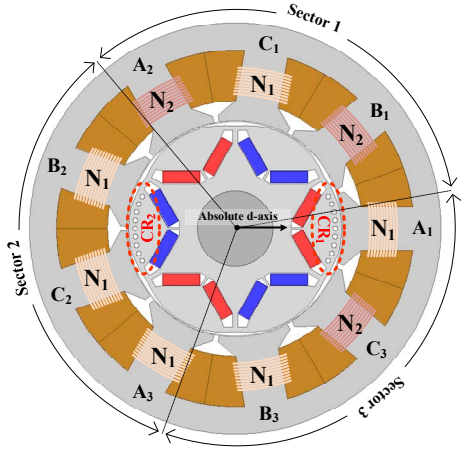

(a) Cross-sectional diagram.

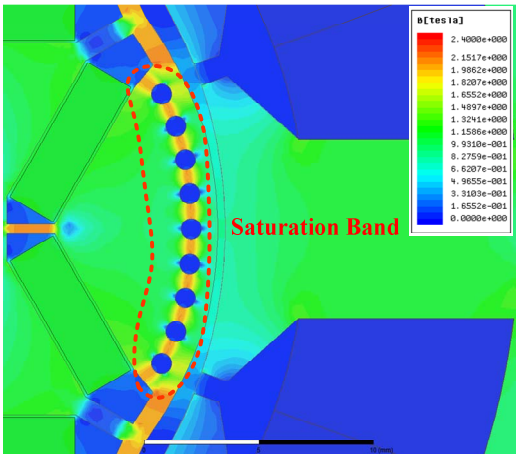

(b) Magnetic flux density distribution at CR1.

Figure 3. Hole-type design.

II. CONVENTIONAL METHOD [5]

A. Conventional Motor Design

Fig. 1 shows cross-sectional diagram of the conventional design of IPMSM with absolute rotor position estimation capability [5]. For realization of the absolute position estimation capability, both stator and rotor was designed to be asymmetric. For the stator asymmetry, the coil turn number at B_1, A_2, and C_3 is N_2 and the other coils are wound with N_1 (N_2>N_1). And two trenches are dug on a specific spot of the rotor for the rotor asymmetry. Absolute d-axis denoted in Fig. 1 synchronously rotates with trenched pole of the rotor. By the interaction of stator and rotor asymmetries, L_{ds} is modulated according to θ_{rm}. In principle, L_{ds} becomes smaller when the absolute d-axis is aligned to higher-turn coil. More detailed explanation of about it is in [5]. Injecting high frequency voltage to d-axis, L_{ds} can be reflected to the induced d-axis current. Fig. 2 shows experimentally measured current profile by injecting 140V, 5kHz square wave voltage. In the figure, the current magnitudes at 40˚, 120˚, and 320˚ in mechanical angle are larger than those at the other positions.

B. Conventional Absolute Position Estimation Algorithm

To get clear information from current magnitude, absolute d-axis should be aligned to stator coils. Thus there are 9 possible alignment positions where stator coils are located. Based on the profile of the induced current, mechanical 360° can be divided by 3 sectors as denoted in Fig. 1. Each sector can be characterized by the phase where induced current is largest. Measuring the magnitude of the current ripple at three positions and finding out the phase where induced current is largest, the mechanical sector can be identified. Assuming that θ_r is already known by basic sensorless control algorithm, θ_{rm} can be estimated by (1), where Δ_{Sector} indicates the difference of sector numbers between the sector number from the initial guess and that after the identification.

$$\hat{\theta}_{rm} = \hat{\theta}_r / 3 + \frac{2\pi}{PP} \cdot \Delta_{Sector} \tag{1}$$

Although the absolute position can be clearly estimated in the conventional motor design, the initial motion of the rotor was inevitable for the sector identification. Since the rotor should be aligned to three different positions respectively, it

978-1-4799-5784-2/14/$31.00©2014 IEEE

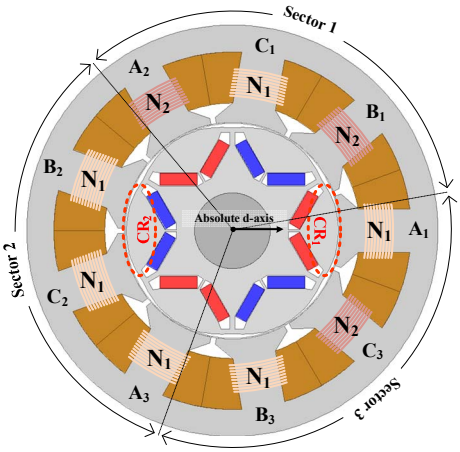

(a) Cross-sectional diagram.

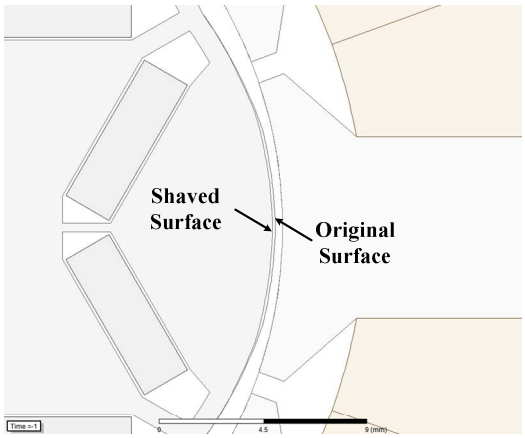

(b) Shaved rotor surface at CR1.

Figure 4. Shaving-type design.

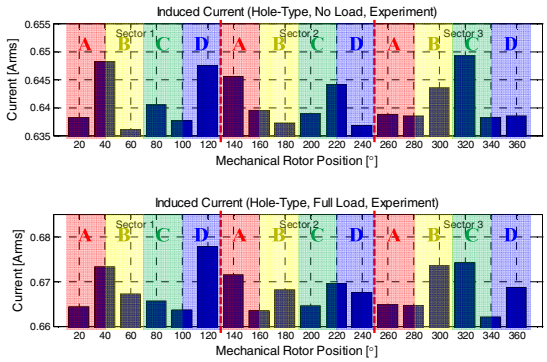

Figure 5. Induced current profiles (hole-type design).

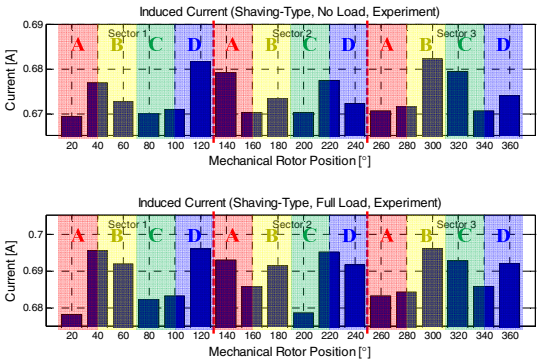

Figure 6. Induced current profiles (shaving-type design).

asked for 100° initial stroke of the rotor in mechanical angle. This large initial stroke of the rotor would be unacceptable in robot and machine tool applications.

III. PROPOSED METHOD

A. Proposed Motor Designs

Fig. 3(a) and 4(a) show proposed motor designs, namely, hole-type and shaving-type design. The same winding method with the conventional design in Fig. 1 is used in both designs. In the figures, N_2 is larger than N_1. Contrast to the conventional design, two characteristic regions denoted as CR_1 and CR_2 are implemented in the rotor. In hole-type design, small holes are dug in two sides of the rotor. In shaving-type design, two sides of the rotor are slightly shaved. In both designs, their characteristic regions form high reluctance parts in magnetic flux path. As shown in Fig. 3(b), the region of the rotor core between the holes is saturated due to narrowed flux path, which finally increases the reluctance of the flux path crossing CR_1. In case of shaving-type design, increased air gap at CR_1 and CR_2 contribute to the high reluctance. In the proposed designs, both CR_1 and CR_2 can be aligned to stator coils. Thus there are eighteen alignment positions, namely, 0°, 20°, …, 340°. Similar to the conventional design, L_{ds} becomes smaller when CR_1 or CR_2 is aligned to higher-turn coil. For example, CR_2 is aligned to C_2 at 20° and CR_1 is aligned to B_1 at 40°. Since the turn number of B_1 is higher than that of C_2, L_{ds} is smaller at 40°. Fig. 5 and 6 show current profiles experimentally measured in no load and full load conditions by 140V, 5kHz square wave voltage injection. In the current profiles, modulated L_{ds} is reflected to the magnitude of the current ripple. The current ripple at 40° is larger than that at 20° because L_{ds} is smaller at 40°. The current profiles are used as database for identifying the mechanical sector.

B. Proposed Absolute Position Estimation Algorithm

From the variation of the current ripple in Fig. 5 and 6, mechanical 360° can be divided into three mechanical sectors denoted as sector 1, 2, and 3. And each mechanical sector can be divided into four electrical sub-sectors denoted as A, B, C, and D. Each of the four sub-sectors spans 90° in electrical angle. Fig. 7 shows initial sector identification procedure. At initial startup, θ_r is estimated by signal injection sensorless control and the initial sub-sector can be found. Then the absolute d-axis is aligned to two nearby positions and the magnitudes of d-axis current ripples at those positions are measured. Alignment positions according to the sub-sector

978-1-4799-5784-2/14/$31.00©2014 IEEE

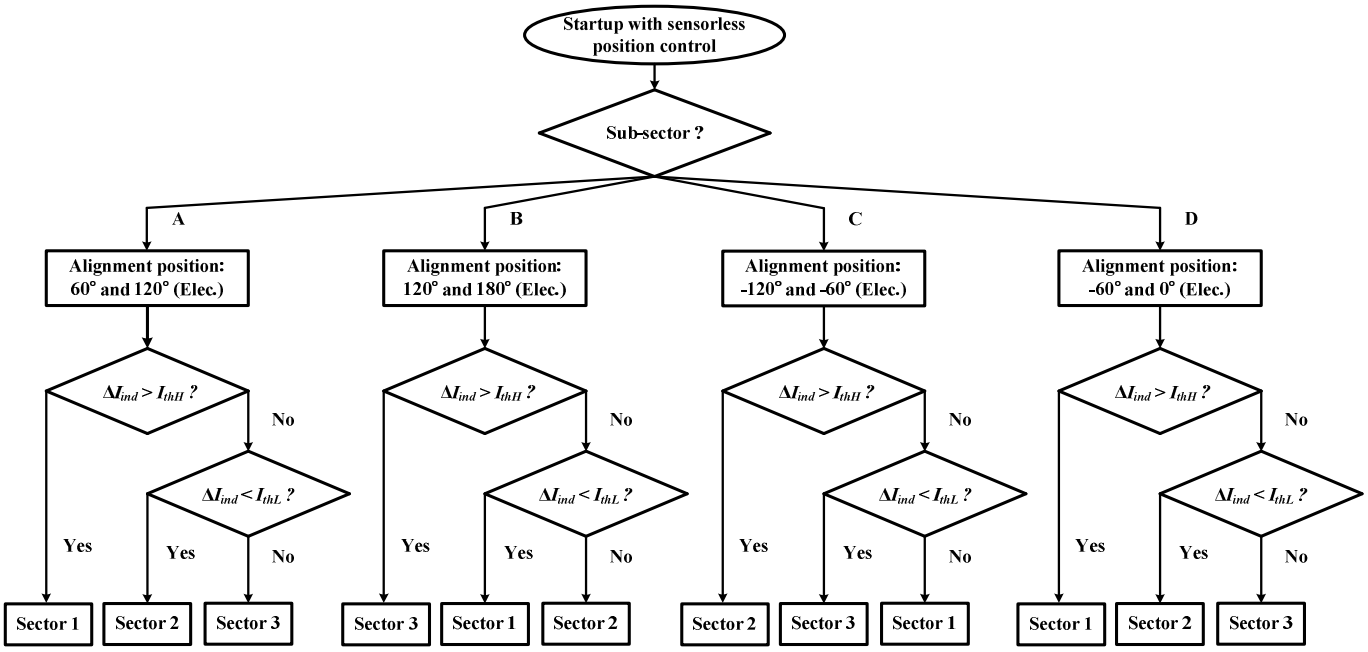

Figure 7. Flowchart of initial sector identification procedure.

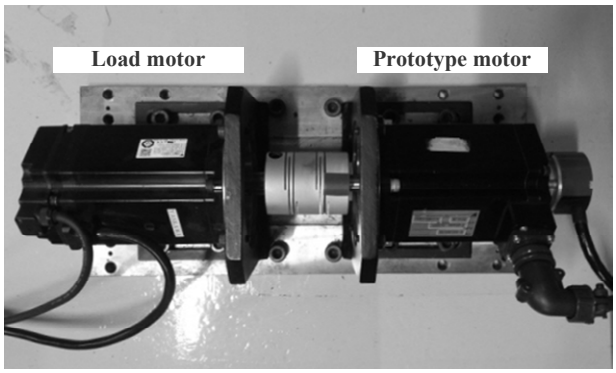

Fig. 8. M-G set.

information are specified in Fig. 7. After that, the difference of induced currents at two alignment positions denoted as ΔI_{ind} is calculated. The mechanical sector can be solely determined after comparing ΔI_{ind} with I_{thH} and I_{thL}, where I_{thH} and I_{thL} indicate pre-set thresholds based on the database of the experimentally measured current profiles obtained by off-line test. Finally, θ_{rm} can be estimated by (1). Using this algorithm, the initial stroke of the rotor can be reduced to 30° in mechanical angle even in the worst case.

IV. Experimental Results

Two motor designs in Fig. 3 and 4 are constructed for experimental test. Fig. 8 shows the M-G set for the experimental verification of the design and control schemes. Fig. 9 shows experimental results. In Fig. 9(a), hole-type motor starts up at initial position -135° which is included in sector 2. After two alignments, sector is identified by comparing ΔI_{ind} with I_{thH} and I_{thL}. Since initially guessed sector was also 1, there is no need to correct $\hat{\theta}_{rm}$. In Fig. 9(a), hole-type motor starts up at initial position -135° which is included in sector 2. After two alignments, sector is identified by comparing ΔI_{ind} with I_{thH} and I_{thL}. Since the identified sector number is different from initially guessed one, $\hat{\theta}_{rm}$ is corrected by subtracting 120° from it. In Fig. 9(c), shaving-type motor starts up at initial position 45° which is included in sector 1. In the same way, sector is identified by comparing ΔI_{ind} with I_{thH} and I_{thL}. Since initially guessed sector was also 1, there is no need to correct $\hat{\theta}_{rm}$. The proposed algorithm also works with the initial rotor position other than 45° and -135°.

V. Basic Characteristics

Due to the asymmetric structure of the proposed motor design, there is inevitable degradation of basic characteristics. Fig. 10 and 11 show back-EMF and torque characteristics of the prototype motors from FEM simulations. In the figures,

978-1-4799-5784-2/14/$31.00©2014 IEEE

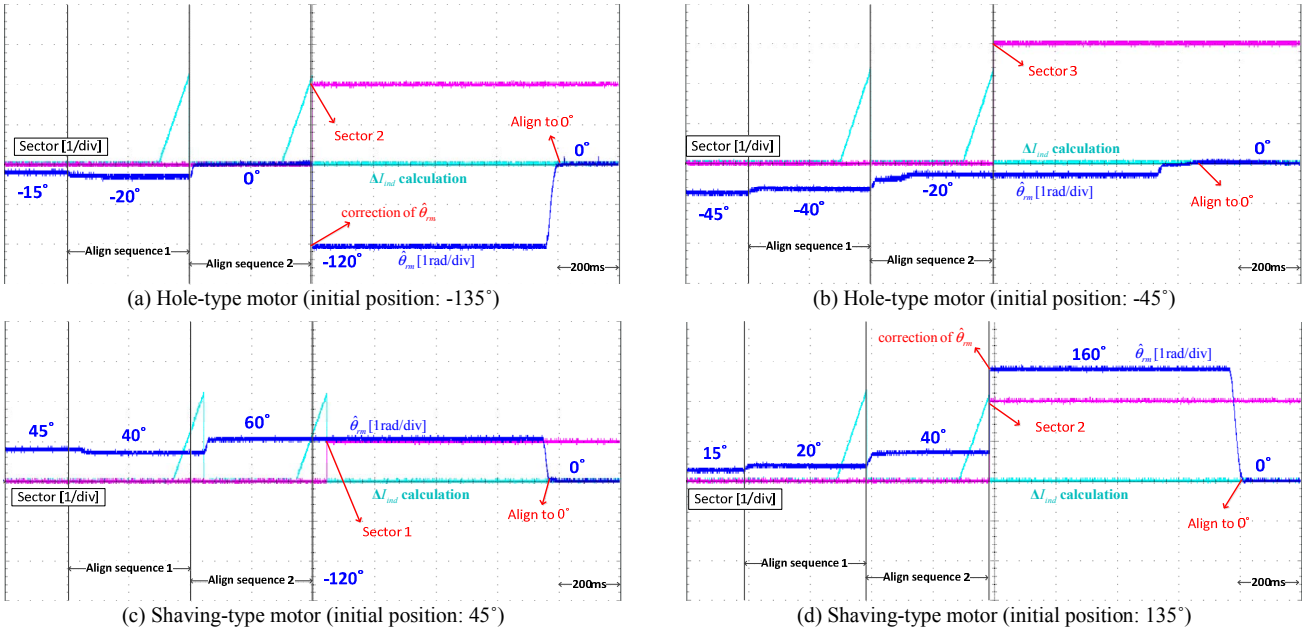

(a) Hole-type motor (initial position: -135˚)

(b) Hole-type motor (initial position: -45˚)

(c) Shaving-type motor (initial position: 45˚)

(d) Shaving-type motor (initial position: 135˚)

Figure 9. Experimental results: Initial sector identification.

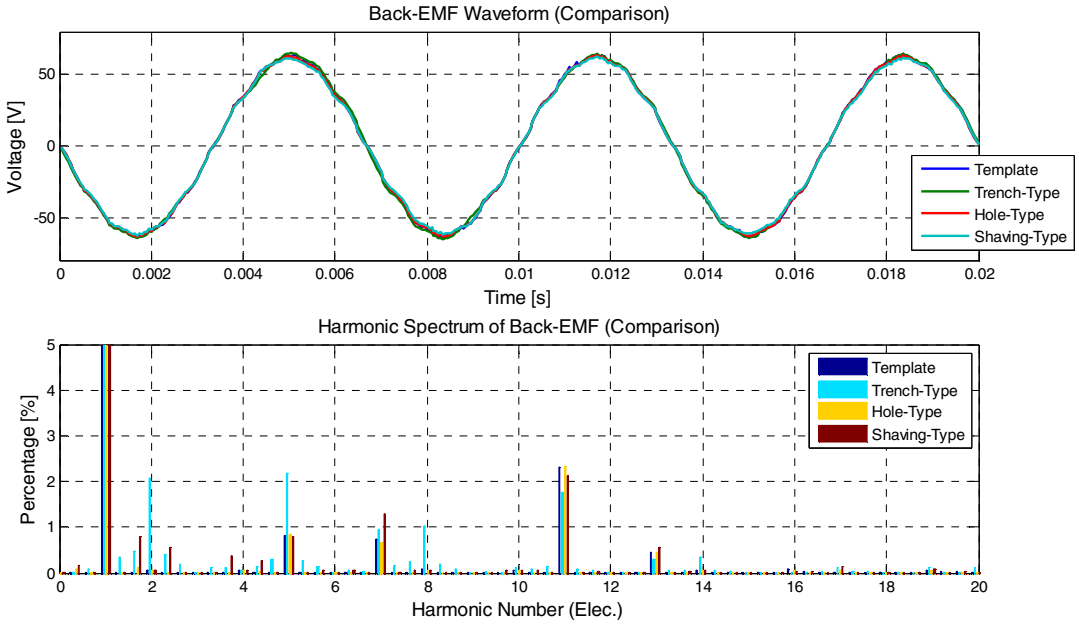

Figure 10. Back-EMF characteristics (zero current, 3000r/min).

trench-type design indicates the conventional one in [5]. It is evident that low-order harmonic components of back-EMF and torque waveforms of trench-type design are conspicuously attenuated by the proposed designs. Thanks to smoothened rotor surface of the two designs, their back-EMF and torque qualities are even comparable to those of template design which has no asymmetry in the rotor and the stator.

Fig. 12 shows Unbalanced Magnetic Pull (UMP) characteristics. In the figure, UMP is calculated by Maxwell's stress tensor from magnetic flux density at the mid-air gap between the rotor and the stator [6]-[7]. In the case of trench-type design, the mean and peak to peak ripple of UMP are 47.7Nm and 72.4Nm, respectively. Both mean and ripple of UMP are reduced in the proposed designs; mean value is reduced by 7.1% and peak to peak value is reduced by 24.9%. Note that UMP does not rotate around the axis but strokes because higher-turn coils at the right-top side make more pulling force as shown in Fig. 12.

VI. CONCLUSIONS

In this paper, two new designs of IPMSM for sensorless drive with absolute rotor position estimation capability have been proposed. With two characteristic regions of the rotor, the number of alignment positions can be doubled. And applying the sector identification algorithm utilizing pre-set threshold values, the initial stroke of the rotor, which was 100 ˚ in the

978-1-4799-5784-2/14/$31.00©2014 IEEE

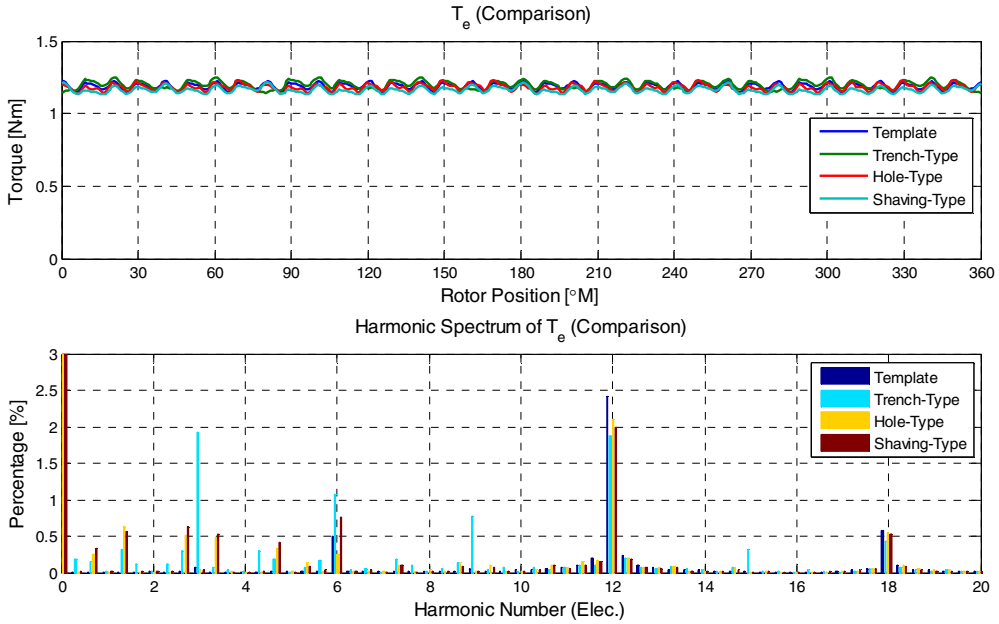

Figure 11. Torque characteristics (full load).

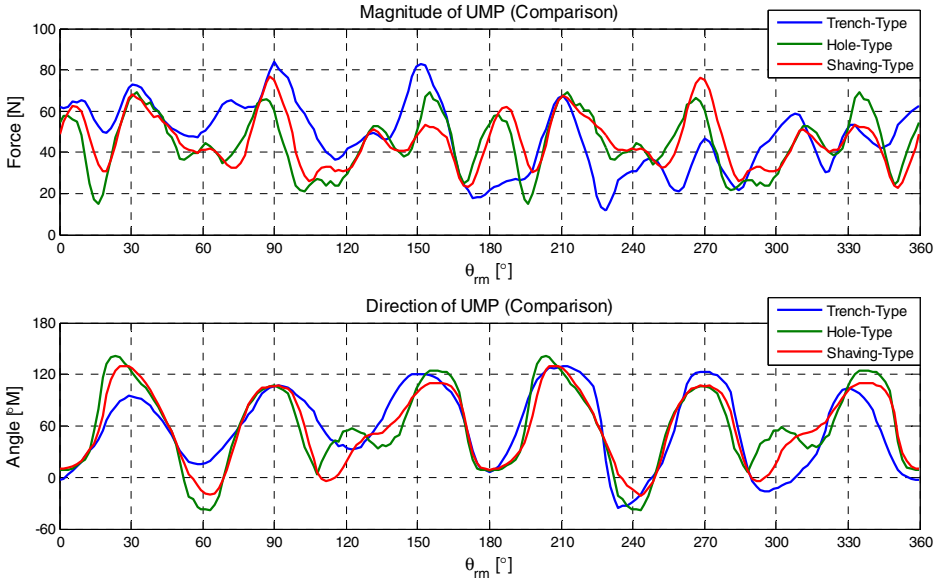

Figure 12. UMP characteristics (full load).

conventional design, has been reduced to 30˚ in mechanical angle. Moreover, basic characteristics including back-EMF, torque, and UMP are remarkably improved from the conventional design.

REFERENCES

[1] P. L. Jansen and R. D. Lorenz, "Transducerless position and velocity estimation in induction and salient AC machines, " *IEEE Trans. Ind. Appl.*, vol. 31, no. 2, pp. 240-247, Mar./ Apr. 1995.

[2] J. I. Ha, and S. K. Sul, "Sensorless field-orientation control of an induction machine by high-frequency signal injection," *IEEE Trans. Ind. Appl.*, vol. 35, no. 1, pp. 45-51, Jan./Feb. 1999.

[3] Y. D. Yoon, S. K. Sul, S. Morimoto, and K. Ide, "High bandwidth sensorless algorithm for AC machines based on square-wave-type voltage injection," IEEE Trans. Ind. Appl., vol. 47, no. 3, pp. 1361-1370, May/Jun. 2011.

[4] A1000 Drive [Online]. Available: http://www.yaskawa.com/site/products.nsf/products/Industrialb%20AC%20Drives~A1000.html

[5] Y. C. Kwon, S. K. Sul, N. A. Baloch, S. Murakami, S. Morimoto, "Design and control of IPMSM sensorless drive for mechanical rotor position detection capability," *Emerging and Selected Topics in Power Electronics, IEEE Journal of* , in press.

[6] G. H. Jang, J. W. Yoon, N. Y. Park, and S. M. Jang, "Torque and unbalanced magnetic force in a rotational unsymmetric brushless DC motors," IEEE Trans. Ind. Magn., vol. 32, no. 5, pp. 5157-5159, Sept 1996.

[7] Z. Zhu, M. Jamil, and L. Wu "Influence of slot and pole number combinations on unbalanced magnetic force in PM machines with diametrically asymmetric windings," IEEE Trans. Ind. Appl., vol. 49, no. 1, pp. 19-30, Jan./Feb. 2013.

978-1-4799-5784-2/14/$31.00©2014 IEEE